

Low energy peripheral scaling in Nucleon-Nucleon scattering and uncertainty quantification

I. Ruiz Simo,^{*} J.E. Amaro,[†] and E. Ruiz Arriola[‡]

Departamento de Física Atómica, Molecular y Nuclear and Instituto Carlos I de Física Teórica y Computacional, Universidad de Granada, E-18071 Granada, Spain

R. Navarro Pérez[§]

Institute of Nuclear and Particle Physics and Department of Physics and Astronomy, Ohio University, Athens, OH 45701, USA

(Dated: November 14, 2018)

We analyze the peripheral structure of the nucleon-nucleon interaction for LAB energies below 350 MeV. To this end we transform the scattering matrix into the impact parameter representation by analyzing the scaled phase shifts $(L + 1/2)\delta_{JLS}(p)$ and the scaled mixing parameters $(L + 1/2)\epsilon_{JLS}(p)$ in terms of the impact parameter $b = (L + 1/2)/p$. According to the eikonal approximation, at large angular momentum L these functions should become an universal function of b , independent on L . This allows to discuss in a rather transparent way the role of statistical and systematic uncertainties in the different long range components of the two-body potential. Implications for peripheral waves obtained in chiral perturbation theory interactions to fifth order (N5LO) or from the large body of NN data considered in the SAID partial wave analysis are also drawn from comparing them with other phenomenological high-quality interactions, constructed to fit scattering data as well. We find that both N5LO and SAID peripheral waves disagree more than 5σ with the Granada-2013 statistical analysis, more than 2σ with the 6 statistically equivalent potentials fitting the Granada-2013 database and about 1σ with the historical set of 13 high-quality potentials developed since the 1993 Nijmegen analysis.

PACS numbers: 03.65.Nk, 11.10.Gh, 13.75.Cs, 21.30.Fe, 21.45.+v

Keywords: NN interaction, nucleon-nucleon phase-shifts, peripheral scaling, long-range correlations

I. INTRODUCTION

The analysis of NN scattering has been a field of intensive research since it provides a good starting point to constrain NN interactions in Nuclear Physics. The mid-range distance region, that proves to be crucial for nuclear binding studies, can so far most accurately be determined by direct fits to NN scattering data. However, unfortunately, this region is not tightly constrained by low energy scattering data, typically below $T_{\text{LAB}} = 350$ MeV. Moreover, the inclusion of well-known long distance effects, such as charge dependent one pion exchange (CD-OPE) interaction, Coulomb, vacuum polarization, relativistic and magnetic moments effects prove crucial for extracting the needed mid-range component from standard χ^2 -fits to the abundant np and pp scattering data at those energies. These fits provide statistically significant confidence that the difference between theory and experiment is a fluctuation whose nature (usually a gaussian) can be determined. This requirement to validate the partial wave analysis (PWA) has been emphasized since the early days (see e.g. [1–3] for reviews and references therein) and was scrupulously followed by the Nijmegen group [4] and the subsequent NijmI, NijmII, Reid93 [5], AV18 [6], CD Bonn [7] and Spectator [8] potentials. The statistical high-quality of these 7 nuclear potentials —potentials with a high-statistical confidence and a corresponding $\chi^2/\nu \sim 1$ — was possible due to the implementation of the small but crucial long-distance effects mentioned

above. These effects were missing in many previous analyses and lead to low statistical significance [9, 10]. The most recent analysis [11, 12] accomplished a 3σ -selfconsistent selected pp+np database involving 6713 data and normalizations in the LAB energy range between 1 eV for np and 338 KeV for pp and a maximum of 350 MeV for both np and pp¹. This has lead to the new 6 Granada potentials denoted as DS-OPE [11, 12], DS- χ TPE [13, 14], SOG-OPE [15], SOG- χ TPE, DS- Δ BO and SOG- Δ BO [16].

In this paper we will focus in analyzing thoroughly the long distance behavior of the NN interaction characterized by peripheral scattering. We will also consider some informative tests which set important and tight constraints on phase-shifts with large angular momentum on the light of these 13 high-quality analyses, sharing *exactly* the same long distance CD-OPE and electromagnetic interactions.

Let us first review the long distance structure of the NN potential in a way that our problem can be easily formulated. The functional form of the NN interaction reflects the exchange of the lightest mesons by Yukawa-like interactions. The time-honored OPE potential dominates the longest distance for $r > 3$ fm, and it is given by

$$V_{\text{OPE},pp}(r) = f_p^2 V_{m_{\pi^0},\text{OPE}}(r), \quad (1)$$

$$V_{\text{OPE},nn}(r) = f_n^2 V_{m_{\pi^0},\text{OPE}}(r), \quad (2)$$

$$V_{\text{OPE},np}(r) = -f_n f_p V_{m_{\pi^0},\text{OPE}}(r) - (-)^T 2f_c^2 V_{m_{\pi^\pm},\text{OPE}}(r), \quad (3)$$

^{*} ruizsig@ugr.es

[†] amaro@ugr.es

[‡] earriola@ugr.es

[§] navarrop@ohio.edu

¹ The Granada-2013 database can be downloaded from the website <http://www.ugr.es/~amaro/nndatabase/>.

where T is the isospin of the np pair. Here $V_{m,\text{OPE}}$ is given by

$$V_{m,\text{OPE}}(r) = \left(\frac{m}{m_{\pi^\pm}}\right)^2 \frac{1}{3} m [Y_m(r) \boldsymbol{\sigma}_1 \cdot \boldsymbol{\sigma}_2 + T_m(r) S_{12}], \quad (4)$$

being Y_m and T_m the usual Yukawa functions,

$$Y_m(r) = \frac{e^{-mr}}{mr}, \quad (5)$$

$$T_m(r) = \frac{e^{-mr}}{mr} \left[1 + \frac{3}{mr} + \frac{3}{(mr)^2} \right], \quad (6)$$

where $\boldsymbol{\sigma}_1$ and $\boldsymbol{\sigma}_2$ are the single nucleon Pauli matrices and $S_{12} = 3\boldsymbol{\sigma}_1 \cdot \hat{\mathbf{r}} \boldsymbol{\sigma}_2 \cdot \hat{\mathbf{r}} - \boldsymbol{\sigma}_1 \cdot \boldsymbol{\sigma}_2$ is the tensor operator.

While the pion masses m can be directly determined independently of the NN interaction, the couplings in the CD-OPE potential need consideration of πN or NN scattering processes, which in turn require a PWA. Based on the Granada-2013 database [11], the most accurate determination of the couplings f_N has been reported by a recent analysis [17, 18] with $\chi^2/\nu = 1.025$. One of the reasons why the couplings can be determined so accurately is the fact that tiny changes in the tail provide important modifications in the small angle and low energy observables, which have been accurately measured. This long distance component of the interaction is very compelling but it is formulated in coordinate space and hence it is not directly accessible to experimental determination. Another possibility is given by an *ab initio* computation of the static energy between two point sources made of three quarks with nucleon quantum numbers on the QCD lattice [19, 20], but so far this approach still provides much larger uncertainties for the Yukawa couplings compared with phenomenological approaches based on a PWA.

One way of highlighting the long distance information from NN scattering is to look *a posteriori* at peripheral partial waves with high angular momentum. The peripheral features of strong interactions among elementary particles have been exploited for more than half a century [21] and they were immediately applied to NN interactions in terms of OPE in the Born approximation [22–24]. Tests for NN peripherality and the meson exchange picture have been made at the partial waves level for high angular momenta [25], and within the chiral perturbation theory proposed by Weinberg [26] at different orders [27–31]. One drawback is that in perturbation theory the meson exchange picture provides singular interactions at short distances, where the order of the divergence generally increases with the order of the coupling constant. However, for a given order there is a partial wave with sufficiently high angular momentum where results are finite, so that angular momentum acts as a perturbative regulator. This regularization procedure is very appealing but it requires passing from the physical and measurable momentum transfer \vec{q} to the angular momentum variable L , thus making necessary a PWA including both peripheral and not peripheral partial waves. At this point it is worth reminding that phase-shifts extracted from a PWA *are not* by themselves observables at a given energy, unless a complete set of scattering and polarization observables at that energy is available. Instead, one has mostly incomplete measurements that demand some interpolation procedure.

One should notice that all these peripheral waves studies are somewhat qualitative and they are based on visual comparison to scattering phases extracted from PWA. To our knowledge, the degree of agreement or disagreement has never been quantified. As an illustration, in Fig. 1 we display np phase-shifts $\delta_{JLS}^{(i)}$ and mixing angles $\epsilon_{JLS}^{(i)}$ for all partial waves with $J \leq 5$ for 13 realistic interactions and in the conventional fashion. We do so for 13 high-quality determinations, but instead of plotting 13 different lines we present a band containing all of them, namely for any energy we take the interval $\min_i \delta_{JLS}^{(i)} \leq \delta_{JLS} \leq \max_i \delta_{JLS}^{(i)}$ and similarly for $\epsilon_{JLS}^{(i)}$. All these interactions share the *same* CD-OPE tail as the dominant feature above 3 fm, and the discrepancies reflect the differences in the interactions below 3 fm, yet fitting the data in a statistically significant manner by the time they were developed. Besides, from the spread observed in all of them and the fact that higher partial waves produce smaller phase-shifts, it is not obvious which LSJ channels can be compared for the *same* range of energies and to *what extent* are these differences significant.

The purpose of the present paper is threefold. First, we present a *peripheral plot*, a universality pattern for the peripheral waves in terms of the impact parameter, suggested by the eikonal approximation. This peripheral plot turns out to be very informative regarding the relevant scales in NN interaction, and how many partial waves are directly intertwined. This is in contrast to the usual plots of phase-shifts in each partial wave as a function of the energy, where this information is, in fact, hidden. Second, we make a clean-cut *quantitative* discussion on the role played by different mid-range interactions on the higher L partial waves. Third, we visualize both statistical as well as systematic errors (see also [16]), and we also single out which phase-shifts behave as outliers when compared to well-established high-quality potentials.

The paper is organized as follows. In Section II we discuss the meaning of "elementariness" in NN interactions as a help to introduce the corresponding impact parameter. In Section III we introduce the peripheral plot in the light of the eikonal approximation, which requires consideration of coupled channels. We illustrate the scaling features of the OPE interaction when treated in perturbation theory. In Section IV we show that scaling indeed works for realistic high-quality interactions when the uncertainties are taken into account. In Section V we use the peripheral plot as well as the corresponding statistical and systematic uncertainties as a quantitative test for two important determinations of peripheral phase-shifts. Finally, in Section VI we summarize our results and present our main conclusions. Technical details are further elaborated in Appendices A, B and C.

II. IMPACT PARAMETER AND EFFECTIVE ELEMENTARINESS

Meson exchange forces such as CD-OPE, Eqs. (1-3), play a similar role as van der Waals interactions in molecular physics: they correspond to the interaction between elementary point-like particles. Nucleons are composite particles with size $\sim a$. This will modify Eqs. (1-3) for $r \lesssim r_c \sim 2a$.

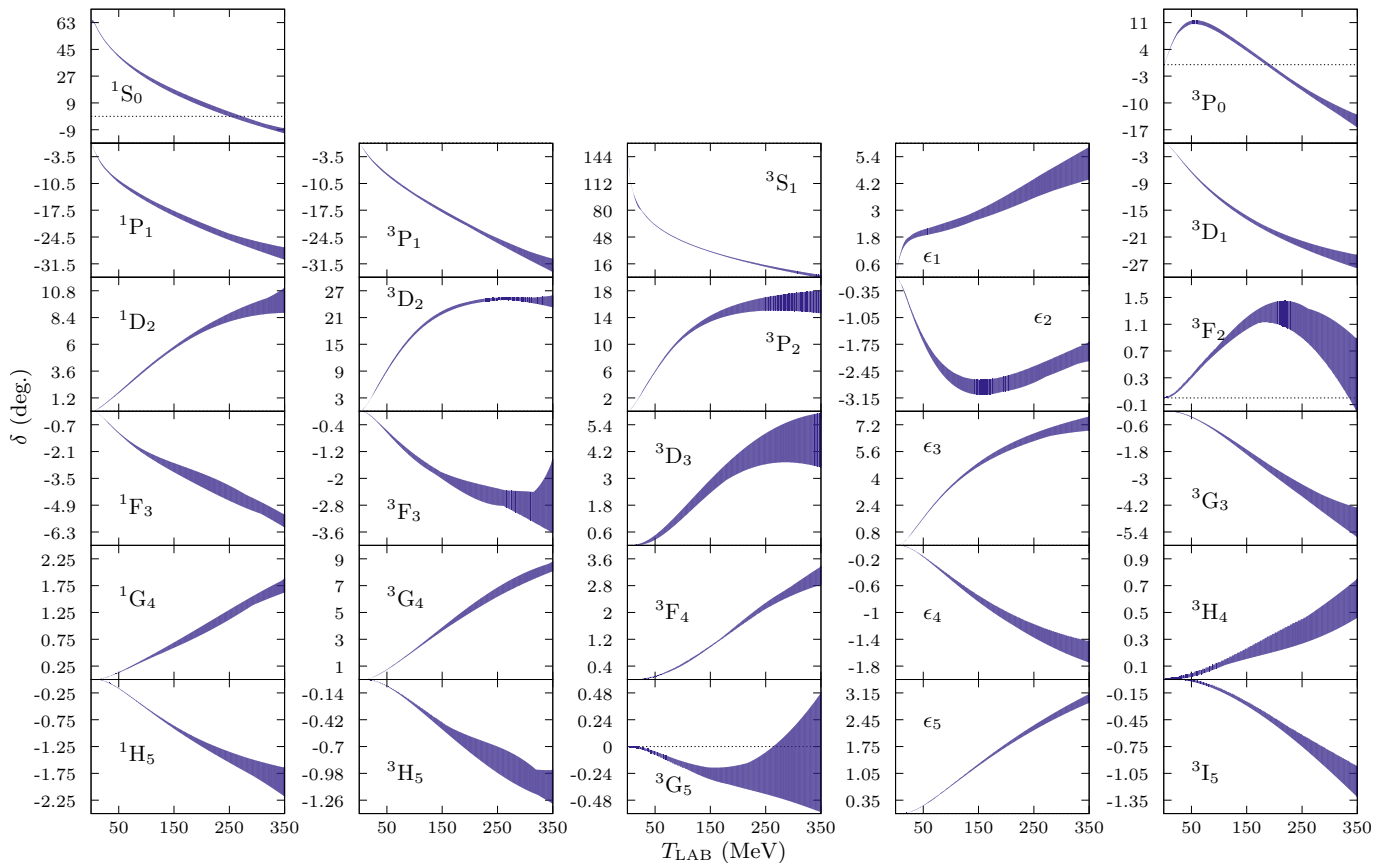


FIG. 1. Neutron-proton phase-shifts (and mixing angle) bands between $\min \delta_i$ and $\max \delta_i$ including 13 high statistical quality potentials with the same CD-OPE tail in all partial waves with $J \leq 5$ as a function of the LAB energy. We consider the Nijmegen PWA [4], Nijm I, Nijm II Reid93 [5] the AV18 [6], CD Bonn [7], Spectator [8], and the recent 6 Granada potentials denoted as DS-OPE [11, 12], DS- χ TPE [13, 14], SOG-OPE [15], SOG- χ TPE, DS- Δ BO and SOG- Δ BO [16].

L	$T_{\text{LAB}}^{\text{max}}$ (MeV) ($b_{\text{eff}} > r_c = 1.8\text{fm}$)	$T_{\text{LAB}}^{\text{max}}$ (MeV) ($b_{\text{eff}} > r_c = 3\text{fm}$)
0	6.4	2.3
1	57.5	20.7
2	159.9	57.6
3	313.5	112.9
4	518.3	186.6
5	774.2	278.7
6	1081.4	389.3

TABLE I. Maximum LAB energies for partial waves not intruding below the distances $b_{\text{eff}} = b/\sqrt{2} > r_c = 1.8\text{fm}$ and $b_{\text{eff}} > r_c = 3\text{fm}$

For instance, the electromagnetic interaction between protons requires consideration of charge distribution by means of a form factor, but it reduces to the Coulomb potential e^2/r for $r \gtrsim 1.8\text{ fm}$ [17]. Microscopically, regulated OPE and TPE follow also a similar pattern, i.e, beyond an elementariness radius, the interactions correspond to point-like particles.

In previous works we have advocated a coarse grained approach [12, 32, 33] for the unknown interaction below the elementariness radius $r_c = 3\text{ fm}$ that gives the best quality fit to NN data below a laboratory (LAB) energy of 350 MeV [11]. This maximum energy corresponds to maximal CM momen-

tum $p_{\text{max}} \sim \sqrt{Mm\pi}$. The coarse grain is based on the idea that, for a fixed angular momentum L , the NN interaction is efficiently sampled at radial points located at a relative distance $\Delta r \sim 1/p_{\text{max}}$.

Within a semi-classical approach the relation between the CM momentum p , the impact parameter b and the angular momentum L is given by²

$$bp = L + \frac{1}{2}. \quad (7)$$

Strictly speaking, the impact parameter is not an observable except at high energies, but we can use it as a convenient variable. Note that for a quantized L , and for a fixed energy, we have $\Delta b = 1/p$, in agreement with the radial coarse grained interval Δr . Better semi-classical approximations provide suitable corrections to the leading behavior, Eq. (7). In any case, Eq. (7) provides a sensible way to define when a given partial wave can be regarded as peripheral, and this has to do with the

² Note that we are making $L(L+1) \rightarrow (L+1/2)^2$ motivated by the well-known Langer modification to ensure the correct $\sim r^{L+1}$ short distance behavior of the WKB wave function (see e.g. [34]).

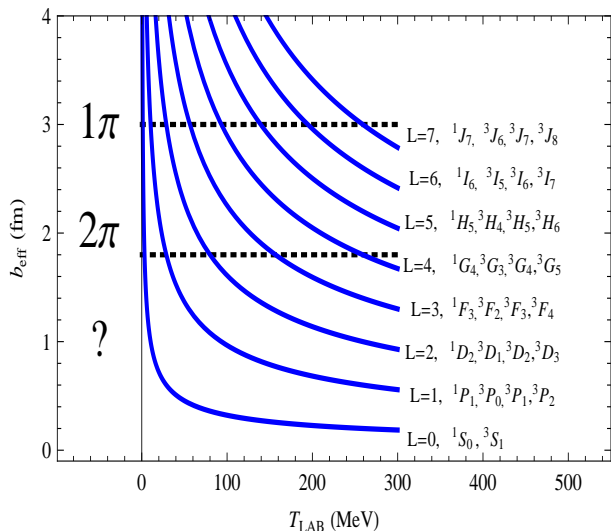


FIG. 2. Effective impact parameter $b_{\text{eff}} = b/\sqrt{2}$ as a function of the LAB energy for different partial waves according to their angular momentum L and the formula $bp = (L+1/2)$ with $T_{\text{LAB}} = 2p^2/M_N$. This probes the region of a short distance potential $V_{\text{Short}}(r)$ which vanishes *above* a certain distance (see main text). The horizontal dotted lines represent the distances above which the NN potential is described by pion exchanges in the Granada analyses [11–15]. Here $V_{NN}(r) = V_{1\pi}(r)$ for $r > r_c = 3$ fm and $V_{NN}(r) = V_{1\pi}(r) + V_{2\pi}(r)$ for $r > r'_c = 1.8$ fm.

spanned range of impact parameters, where we know for certain that the long range force is produced by pion exchange.

Based on the Granada-2013 np+pp database [11], we carried out comprehensive and statistically consistent fits allowing to clearly identify the regions where there is only OPE (CD-OPE) [11, 17, 18] and one+two pion-exchange (CD-OPE+TPE) [13, 35, 36], namely

$$V_{NN}(r) = V_{1\pi}(r), \quad r > r_c = 3.0 \text{ fm} \quad (8)$$

$$V_{NN}(r) = V_{1\pi}(r) + V_{2\pi}(r), \quad r > r'_c = 1.8 \text{ fm} \quad (9)$$

For distances below $r'_c = 1.8$ fm, finite nucleon size effects (3π exchange, heavier mesons or quark exchange) become important and difficult to disentangle. We effectively incorporate these short distance components as a sum of delta-shells separated by $\Delta r = 0.6$ fm, with strengths fitted to the np and pp scattering database. Attempts to extend TPE below that distance either produce too large χ^2 values or unnaturally large low energy constants, and hence they had to be ruled out [36, 37]. Within the EFT framework this means that counter-terms have a range smaller than r'_c .

The above discussion implies that the short distance component (the delta-shells) of the potential has a sharp end, i.e. $V_{\text{Short}}(r) = 0$ for $r > r'_c$ [13, 35, 36] or for $r > r_c$ [11, 17, 18], depending on the analyses. If we denote the corresponding phase-shifts by $\delta_{L,\text{Short}}(k)$, then the partial wave expansion of the scattering amplitude corresponding to this short distance component (we assume a central potential to simplify the dis-

ussion) can be written as

$$f_{\text{Short}}(\theta) = \sum_{L=0}^{\infty} (2L+1) \frac{e^{2i\delta_{L,\text{Short}}(k)} - 1}{2ik} P_L(\cos\theta). \quad (10)$$

The analogous expansion for the total cross section is then

$$\sigma_{\text{Short}} = \frac{4\pi}{k^2} \sum_{L=0}^{\infty} (2L+1) \sin^2 \delta_{L,\text{Short}}(k). \quad (11)$$

Based on Eq. (7) with the impact parameter b replaced by the sharp end of the short distance component of the potential (r'_c or r_c), one would expect that there is an effectively maximum angular momentum for each energy, $L_{\text{max}} \sim kr'_c$, beyond which short distance phase-shifts become negligible, thus truncating the infinite series of Eqs. (10) and (11). While this happens for the total cross section, it is not exactly the same for the scattering amplitude $f_{\text{Short}}(\theta)$. In fact, the scattering amplitude at backward angles requires $L_{\text{max}} \sim 2kr'_c$ due to a diffractive effect caused by the sharp boundary. These effects are illustrated in Appendix A for a simple spherical well potential. Likewise, within a semi-classical context one should have vanishing scattering for $b > r'_c$. Actually, this is not so, and phase-shifts vanish only when $b \gtrsim \sqrt{2}r'_c$, essentially due to a diffractive effect which vanishes at very short wavelengths (see also Appendix A for the spherical well potential case). Therefore, it is useful to define an effective impact parameter, $b_{\text{eff}} = b/\sqrt{2}$, which complies better with the actual situation.

We illustrate in Fig. 2 the effective impact parameter as a function of the LAB energy for fixed L values (Eq. (7)). Some pertinent numerical values are presented in Table I.

The cut radii for OPE and OPE+TPE are shown with horizontal lines. As we clearly see, below pion production threshold, $T_{\text{LAB}} \leq 290$ MeV, all waves with $L = 0, 1, 2, 3$ intrude into the short distance region below the elementariness radius r'_c . This implies that short distance phenomenological components (or equivalently EFT-counterterms, see below) for these partial waves will generally be needed to describe scattering data in addition to the OPE and TPE potentials. Likewise, for this energy we may regard $G, H, I \dots$ waves as truly peripheral. If the LAB energy is reduced to 125 MeV, then the F waves also behave as peripheral and they will need no short distance phenomenological components. This feature has been verified explicitly by comparing the quality of the fits in different scenarios [36, 37].

III. THE PERIPHERAL PLOT

Our present motivation for an universal plot where many partial waves share their long distance content comes from the eikonal approximation. Let us consider the scattering by a *local* potential $V(r)$ independent on the angular momentum³.

³ For the long distance component, the locality and angular momentum assumptions are supported by the particle exchange picture as well as data analyses based on the L -dependent potentials [15, 16], where terms L^2 are non-vanishing only at short distances.

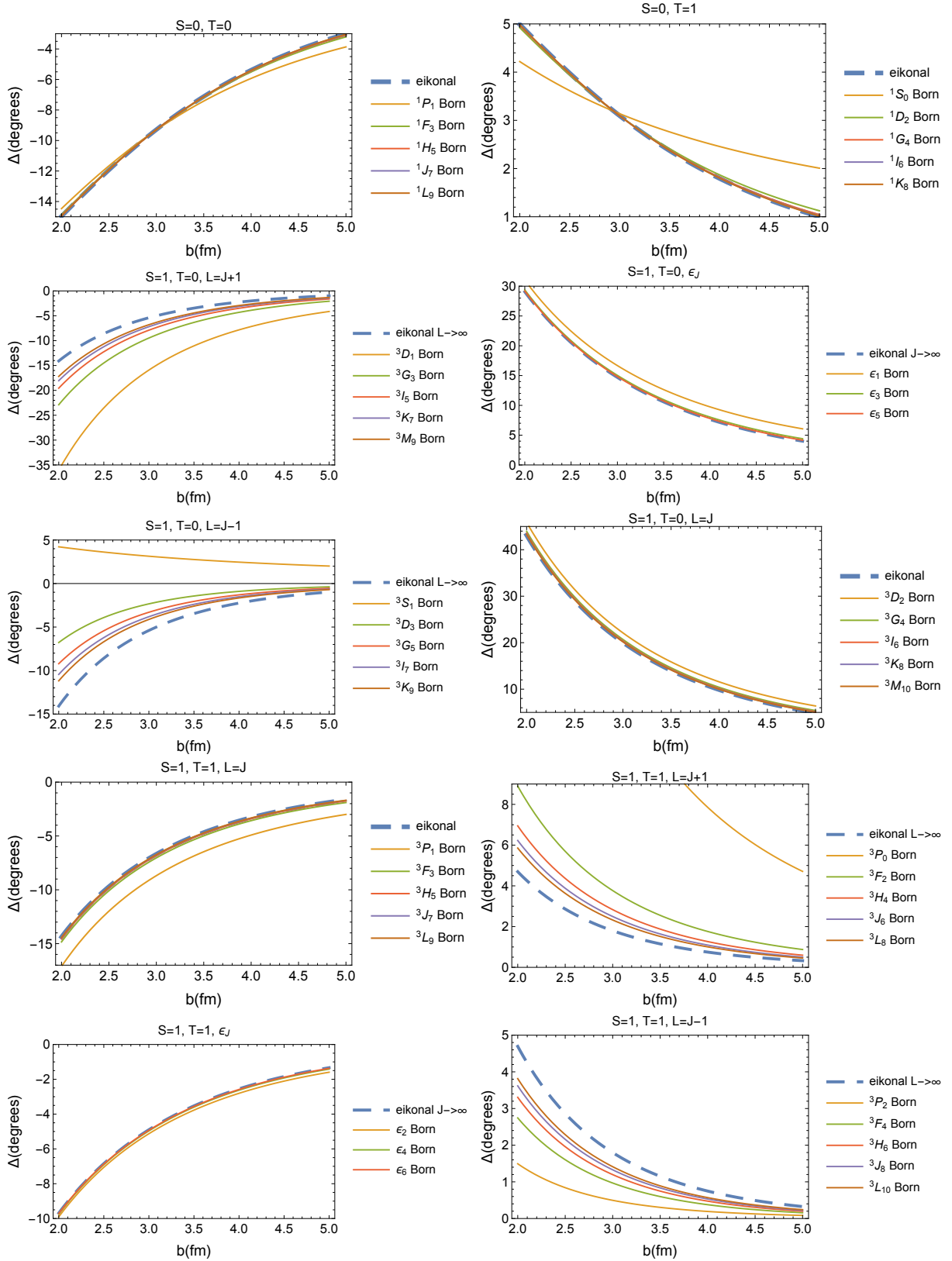


FIG. 3. Scaled phase-shifts $\Delta_{S_L J}$ for the OPE-potential computed in Born and eikonal approximations as a function of the impact parameter b .

The phase-shifts in the eikonal approximation are given by

$$\delta_L(p) = -\frac{M}{2p} \int_b^\infty dr \frac{r}{\sqrt{r^2 - b^2}} V(r). \quad (12)$$

This result also holds in the WKB approximation for a potential much smaller than the centrifugal barrier [34]. In this expression the impact parameter acts as a short distance regulator. The interesting feature of the eikonal approximation is that this property remains true to all orders in the eikonal expansion [38]. This is unlike standard perturbation theory based on expansions in powers of the potential, where this contributes at all points, i.e. $0 \leq r < \infty$, and this becomes critical for singular potentials, like OPE (specially the tensor force) or chiral TPE potentials⁴ (see [39, 40]).

We define the scaled phase-shift as

$$\Delta_L(b) \equiv \left(L + \frac{1}{2}\right) \delta_L(p). \quad (13)$$

Using Eq. (7) and Eq. (12), in the eikonal approximation we get

$$\Delta_L(b) = -\frac{Mb}{2} \int_b^\infty dr \frac{r}{\sqrt{r^2 - b^2}} V(r). \quad (14)$$

Note that according to the eikonal approximation the scaled phase-shift, $\Delta_L(b)$, *only* depends on the impact parameter if the potential $V(r)$ does not depend on the angular momentum. One expects to observe this scaling in the so-called *peripheral plot*, where $\Delta_L(b)$ is represented instead of $\delta_L(p)$. In the real situation encountered in a PWA we expect violations to this scaling behavior only for low partial waves or for small impact parameters. In general, the explicit angular momentum dependence of the tensor interaction induces the most important violation. Nonetheless, in this work we will see that in several cases these relations work rather accurately within the experimental uncertainties.

While the discussion on peripherality for a central potential is rather straightforward, complications arise in presence of the NN tensor force. In particular, a direct eikonal three-dimensional treatment of the tensor force [41], unlike the central force case, generates ambiguities. The alternative discussion based on a WKB approach to coupled channel partial waves [42] provides no way to calculate the mixing parameters ε_{SLJ} . In this work we introduce an alternative approach by using first-order perturbation theory, and then taking the eikonal limit according to the WKB approximation.

Results are particularly simple for the nuclear bar representation and we refer to Appendices B and C for details. In

first-order perturbation theory we have (see Appendix B)

$$\bar{\delta}_{SJJ}(p) = -\frac{M}{p} \int_0^\infty dr [\hat{j}_J(pr)]^2 V_{JJ}^J(r), \quad (15)$$

$$\bar{\delta}_{SLJ}^\pm(p) = -\frac{M}{p} \int_0^\infty dr [\hat{j}_{J\pm 1}(pr)]^2 V_{J\pm 1, J\pm 1}^J(r), \quad (16)$$

$$\bar{\varepsilon}_{SLJ}(p) = -\frac{M}{p} \int_0^\infty dr \hat{j}_{J-1}(pr) \hat{j}_{J+1}(pr) V_{J-1, J+1}^J(r) \quad (17)$$

where $\hat{j}_l(x) \equiv x j_l(x)$ are the reduced spherical Bessel functions. Note that, in the above expressions, the potential contributes everywhere. The $1/r^3$ singularity could be tamed by introducing a short distance cut-off r_c , generating a cut-off dependence which, however, becomes mild⁵ for $J > 2$.

We now define the scaled phase-shifts for $S = 1$,

$$\Delta_{SLJ}^- = (J - 1/2) \bar{\delta}_{SLJ}^-, \quad (18)$$

$$\Delta_{SLJ}^\varepsilon = (J + 1/2) \bar{\varepsilon}_{SLJ}, \quad (19)$$

$$\Delta_{SLJ}^+ = (J + 3/2) \bar{\delta}_{SLJ}^+, \quad (20)$$

in terms of the nuclear bar representation. We then apply the WKB approximation, as shown in Appendix C, obtaining very simple results. For the uncoupled channels Eq. (14) remains valid. In the coupled channels case, Eq. (14) also holds for the diagonal matrix element, so that the only modification comes from the off-diagonal element,

$$\Delta_{SLJ}^\pm(b)_{\text{WKB}} = -\frac{Mb}{2} \int_b^\infty dr \frac{r}{\sqrt{r^2 - b^2}} V_{J\pm 1, J\pm 1}^J(r), \quad (21)$$

$$\Delta_{SLJ}^\varepsilon(b)_{\text{WKB}} = -\frac{Mb}{2} \int_b^\infty dr \frac{2b^2 - r^2}{r\sqrt{r^2 - b^2}} V_{J-1, J+1}^J(r). \quad (22)$$

In Fig. 3 we compare the values of the Δ 's both for the eikonal approximation and the perturbative OPE result. As we see, the scaling holds already for moderate values of the angular momentum J , especially for the uncoupled partial waves and the mixing phases ε_J . In the eikonal calculations shown in Fig. 3 for the coupled channels, the limit $L \rightarrow \infty$ has been taken in the matrix elements of the OPE potential appearing in Eqs. (21) and (22). This is important to get rid of the explicit L -dependence in these matrix elements, due to the presence of the tensor operator S_{12} .

It is also worth noting that the convergence of the scaled phase-shifts for the coupled partial waves computed in the Born approximation with the OPE potential is much slower than in the other waves, as shown in Fig. 3. This effect is, again, due to the explicit L -dependence of the potential matrix elements in these channels. However, we have checked that increasing the angular momentum L , the Born OPE results eventually reach the eikonal curves indicated by the dashed lines in Fig. 3.

⁴ In fact, it was shown in appendix C of Ref. [40] that for potentials more singular than $\frac{1}{r^2}$ at the origin, there is always a finite order in standard perturbation theory where the lowest-lying partial waves give divergent contributions for the phase-shifts, even although the Born approximation was finite for these partial waves.

⁵ However, as shown in Ref. [40] and already commented in the previous footnote, higher-order perturbation theory will reinstate the short distance divergence.

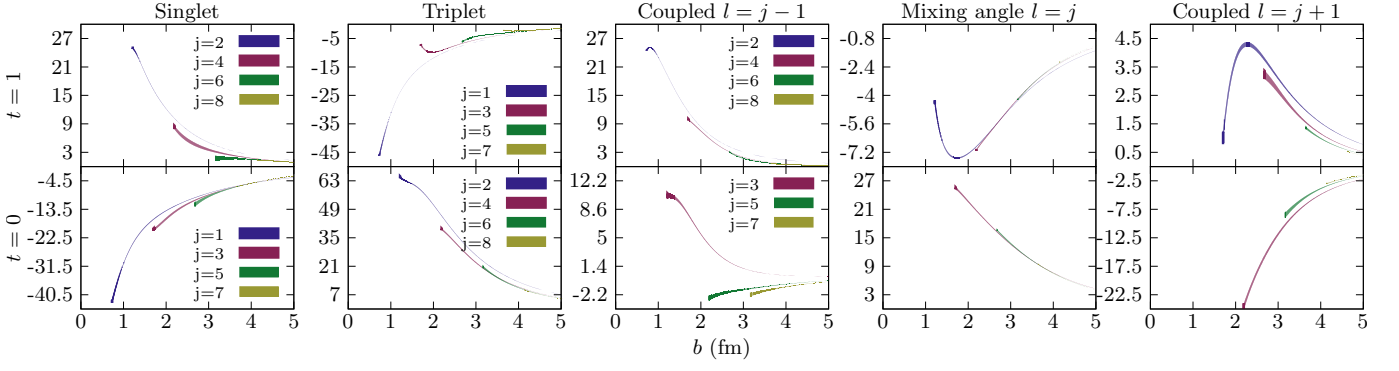


FIG. 4. Peripheral plots for the scaled phase-shifts (in degrees) $(L+1/2)\delta_{SLJ}(p)$ with $L=J, J\pm 1$ and $pb=(L+1/2)$ and mixing angles $(J+1/2)\epsilon_J(p)$ with $pb=(J+1/2)$ as a function of the impact parameter b (in fm). The statistical errors for the DS-OPE PWA are taken from Refs [11, 12].

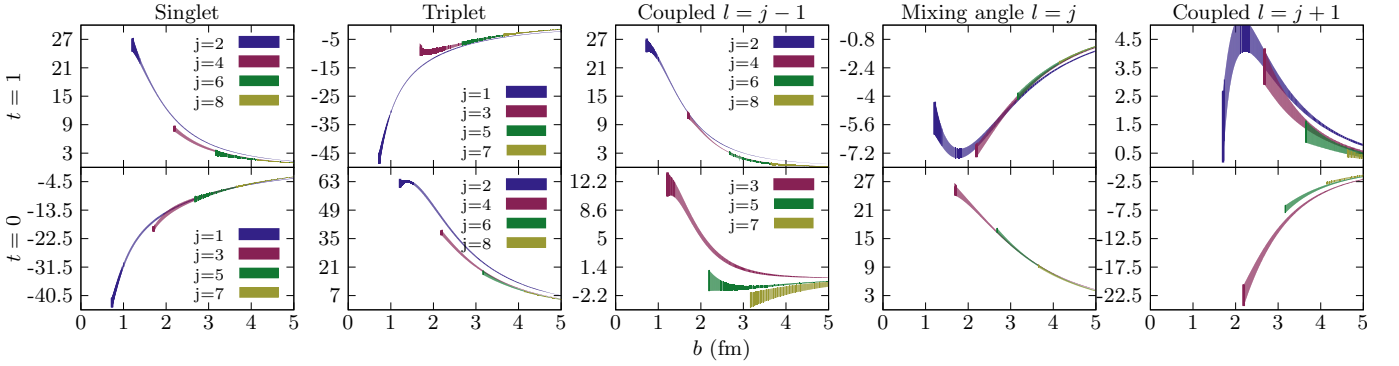


FIG. 5. Same as Fig. 4 but for phase-shifts coming from 13 high-quality fits in all partial waves with $J \leq 5$, as a function of the impact parameter. We show the Nijmegen PWA [4], Nijm I, NijmII, Reid93 [5], the AV18 [6], CD Bonn [7], Spectator [8] and the six Granada potentials denoted as DS-OPE [11, 12], DS- χ TPE [13, 14], SOG-OPE [15], SOG- χ TPE, DS- Δ BO and SOG- Δ BO [16].

IV. PERIPHERAL PLOTS FOR HIGH QUALITY INTERACTIONS

As we have already mentioned, we seek for a more direct relation between the configuration space extension of the potential and the determined phase-shifts. Motivated by the perturbative analysis of the previous section, we show in Fig. 4 the scaled phase-shifts for the DS-OPE potential obtained in the Granada-2013 PWA [11, 12]. All different channels with $J \leq 6$ are shown grouped among uncoupled (singlet and triplet panels) and coupled channels. The three scaled phase-shifts ($\Delta^-, \Delta^e, \Delta^+$) for coupled channels were defined in Eqs. (18–20) and in the figure are labeled with the effective value of the angular momentum applied in the peripheral plot, which is $J-1, J$ and $J+1$, respectively. In the case of the uncoupled channels the value of the angular momentum $L=J$ is used to scale the phase-shifts as defined in Eq. (13).

According to our previous discussion, impact parameters below the elementariness radius $b < r'_c = 1.8$ fm most likely probe nucleon finite size effects and hence we expect the largest deviations in this range, as it can be checked from Fig. 4. The level of scaling is remarkable in the uncoupled channels, where the scaled phase-shifts almost overlap for $L > 2$. In the coupled channels, the scaling violations for the

Δ^\pm have to do with the explicit L -dependence of the diagonal components of the potential. The off-diagonal potential has a weaker L -dependence, resulting in a remarkable degree of scaling of the Δ^e . The panels of Fig. 4 share the same similarities already observed in those of Fig. 3, thus resembling the OPE perturbative treatment of the previous section, but going beyond it by considering all orders.

In Fig. 4 we also display the corresponding statistical error bars. As we see these errors are tiny in the peripheral plot (they are even smaller than a typical line-width). As anticipated in our discussion above, the reason of these very small errors is that, once the f^2 coupling constant is fixed to large accuracy, errors above $b > 1.8$ fm stem only from higher order perturbative corrections beyond the Born approximation. The usefulness of this figure is that, besides packing all phase-shifts for fixed isospin into five separate groups with similar behavior, for data below pion production threshold the range of the potential being probed becomes rather obvious in terms of the impact parameter.

It is also interesting to compare the peripheral plot for some of the available high-quality interactions sharing the *same* CD-OPE potential with the *same* and common coupling con-

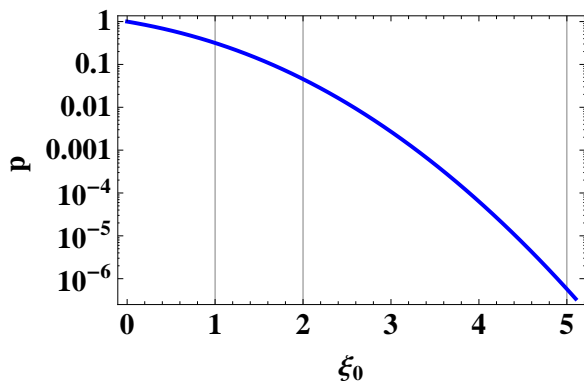


FIG. 6. The probability of *not being an outlier* as a function of the standardized discrepancy value ξ_0 (see main text). We mark the values corresponding to 1,2 and 5 standard deviations.

stant $f^2 = 0.075^6$. They correspond to the Nijmegen PWA results denoted Nijm I, NijmII, and Reid93 [5], the AV18 [6], CD Bonn [7], and Spectator [8] potentials, and to the six Granada potentials denoted DS-OPE, DS- χ TPE, DS- Δ BO, SOG-OPE, SOG- χ TPE and SOG- Δ BO [13–15]. To this end we define the mean and the standard deviation as usual,

$$\text{Mean}(\delta) = \frac{1}{N} \sum_{i=1}^N \delta^i, \quad (23)$$

$$\text{Std}(\delta) = \sqrt{\frac{1}{N-1} \sum_{i=1}^N (\delta^i - \text{Mean}(\delta))^2}, \quad (24)$$

and similarly for the scaled phase-shifts Δ .

In Fig. 5 we show the spreading band of the scaled phase-shifts generated by these different PWA, which describe their contemporary NN scattering database. As we have stressed in Ref. [16], this can be considered as a lower bound on the estimate of the systematic errors as a function of the inter-nucleon distances being explored. The larger errors are concentrated at short distances, and this reflects our lack of knowledge on how the interaction should be parameterized in the short distance region. While the true errors are expected to be larger, in the long distance region they are very small due to the fixed long distance behavior of the potential.

V. PERIPHERAL TESTS AND OUTLIERS

The previous statistical and systematic error bands set very tight constraints on any analysis of peripheral waves and we can use them as a test on the quality of a given interaction and/or scattering amplitude. We will discuss the peripheral plot in two different cases for their particular significance and popularity in quite different contexts: the SAID partial wave

analysis [50] and the recent N5LO calculation of Entem *et al.*, [31]. We will carry out the discussion by conveniently zooming Figs. 4 and 5 by defining a quantitative estimate for a given partial wave. We will consider three different comparisons. Firstly, we compare both analyses to the statistical one carried out in the original paper determining the Granada-2013 database (DS-OPE [11]), which we denote δ_{Gr} and Δ_{Gr} for the phase-shifts and the scaled phase-shifts, respectively. Finally, we also compare the SAID and N5LO analyses to the average of the $N = 6$ Granada potentials, and with the average of the $N = 13$ high-quality potentials mentioned in section IV and plotted in Fig. 5.

Thus we define in the first case the normalized statistical discrepancy

$$\xi^i|_{\text{stat}} = \frac{\Delta^i - \Delta_{\text{Gr}}}{\Delta(\Delta_{\text{Gr}})} = \frac{\delta^i - \delta_{\text{Gr}}}{\Delta\delta_{\text{Gr}}}, \quad (25)$$

corresponding to Fig. 4. In the second and third comparisons, we use Eq. (23) and Eq. (24) with $N = 6$ and $N = 13$, respectively, and we define the normalized systematic discrepancy

$$\xi^i|_{\text{sys}} = \frac{\Delta^i - \text{Mean}(\Delta)}{\text{Std}(\Delta)} = \frac{\delta^i - \text{Mean}(\delta)}{\text{Std}(\delta)}, \quad (26)$$

This quantity measures the deviation of the phase-shifts (Δ_i or δ_i) corresponding to the model i ($=$ N5LO, SAID) with respect to the averaged phase-shifts of the other analyses (either the 6 Granada potentials or the 13 high-quality potentials), divided by their standard deviation. The standardized discrepancies $\xi^i(b)$ will be studied as a function of the impact parameter for the most peripheral partial waves.

It is well known that for any statistical distribution a confidence level p can be defined. In the case of a ξ variable following a normal distribution, the confidence level is the probability that ξ is larger than a fixed value ξ_0

$$p(|\xi| > |\xi_0|) = 1 - \int_{-\xi_0}^{\xi_0} dx \frac{e^{-x^2/2}}{\sqrt{2\pi}}. \quad (27)$$

In the cases $\xi_0 = 1, 2, 3$ one has $p = 0.32, 0.05, 0.01$, corresponding to $1\sigma, 2\sigma$ and 3σ respectively. Thus the probability to obtain a result larger than one-sigma ($\xi > 1$) is 32%, while the probability of it being larger than three-sigmams ($\xi > 3$) is only 1%, so it is statistically very unlikely. Here we understand this p -value as the probability of the corresponding result *not being an outlier*. The situation is pictorially represented in Fig. 6.

A. SAID partial wave analysis

The NN PWA at energies below and well above the pion production threshold has also a long history and a good example of subsequent upgrades is represented by the series of works conducted by Arndt and collaborators [43–48] (see also the GWU database [49]). The most recent GWU fit [50], called SM16, is based on a parameterization [44] with a total number of 147 parameters, fitting all partial wave amplitudes (phases and inelasticities) up to $J = 7$, below 3 GeV and 1.3

⁶ The most recent determination yields $f^2 = 0.0763(1)$ [18] but we prefer to keep the same old value to enhance the long distance equivalence of all potentials.

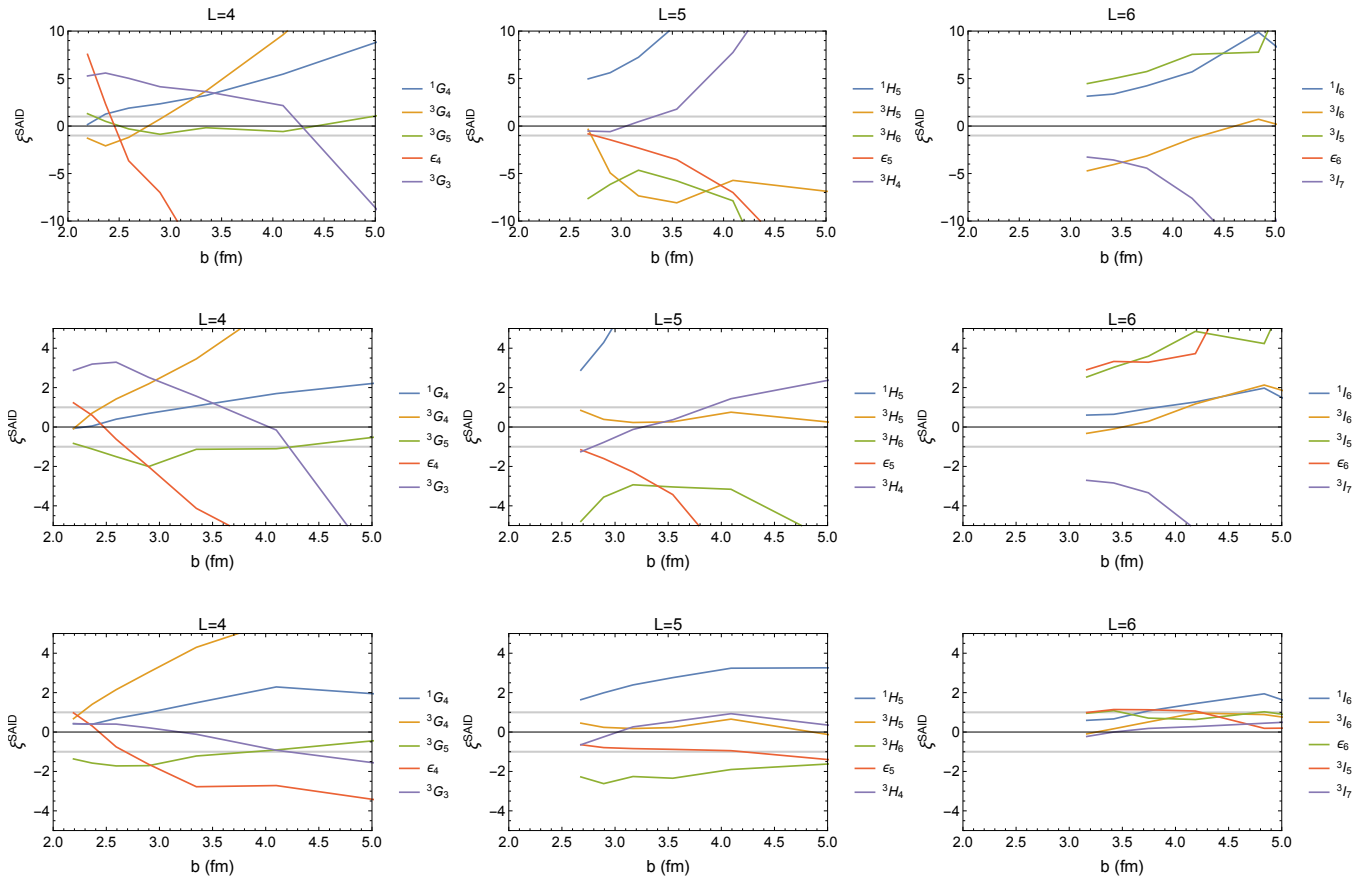


FIG. 7. Comparison of the normalized discrepancy of the SAID NN solution (SM16) [50] with some sets of fits for $L = 4$ (left), $L = 5$ (middle) and $L = 6$ (right) as a function of the impact parameter $b = (L + 1/2)/p$ for energies below $T_{\text{LAB}} = 350$ MeV. Top panels: comparison to the DS-OPE potential [11, 12]. Middle panels: comparison with the average of the 6 Granada-2013 potentials. Bottom panels: comparison with the average of the full set of 13 high-quality potentials. Non-plotted discrepancies are out of range.

GeV of Lab energy for pp and np scattering, respectively. It deals with a large body of 25362-pp data (with $\chi^2 = 48780.9$) and 13033-np data (with $\chi^2 = 26261.0$), which is sufficient for our considerations here. This database is probably the largest one and no data selection was undertaken.

The GWU PWA was carried out up to Lab energy of 3 GeV for the pp case and hence much smaller impact parameters are reached than with the analyses stopping at 350 MeV. On the other hand, this analysis does not incorporate charge dependence in the OPE, nor the small but crucial electromagnetic effects.

In Fig. 7 we plot the normalized discrepancy ξ^{SAID} to the original DS-OPE Granada fit (upper panel), to the average of the six Granada-2013 fits (middle panel) and to the average of the 13 high-quality potentials (bottom panel). We only show the relevant region $b > 2$ fm. Most of the deviations are larger than one sigma, and in some cases they are even larger than 2 or 3 sigmas if compared with the Granada-2013 band. According to these results, the GWU peripheral phase-shifts are outliers, incompatible with the most accurate PWA of the Granada-2013 database. If compared with the full set (bottom panel of Fig. 7), some of the more peripheral waves become more compatible.

In an earlier work [47], the SAID analysis was also carried out in the restricted LAB energy range 0 – 400 MeV (pp+np) and compared to the full energy range results going up to 3 GeV (pp) and 1.3 GeV (np). The 0 – 400 MeV fits, called SP40, used 30+27=57 variable parameters corresponding to $\chi^2/\text{datum} = 4398/3454$ and $\chi^2/\text{datum} = 5415/3831$. These solutions turned out not to be very different from the higher energy fits, called SP00, where the outgoing quality of the fit in the lower 0 – 400 MeV range turned out not to be very different, namely 4593/3454 (pp) and 5371/3831 (np). It was thus concluded that high energy SP00 fits did not degrade the low energy SP40 solutions. We show for comparison the SAID-SP40 solution corresponding to 0 – 400 MeV fits in Fig. 8, and the trends are overall similar to those found in Fig. 7 for the most recent SM16 solution [50].

B. N5LO Chiral Nuclear Forces

Within a modern perspective and following the proposal by Weinberg [26] (see e.g. [51] for a comprehensive review) of implementing a power counting based on a perturbatively rooted effective field theory, chiral symmetry can be im-

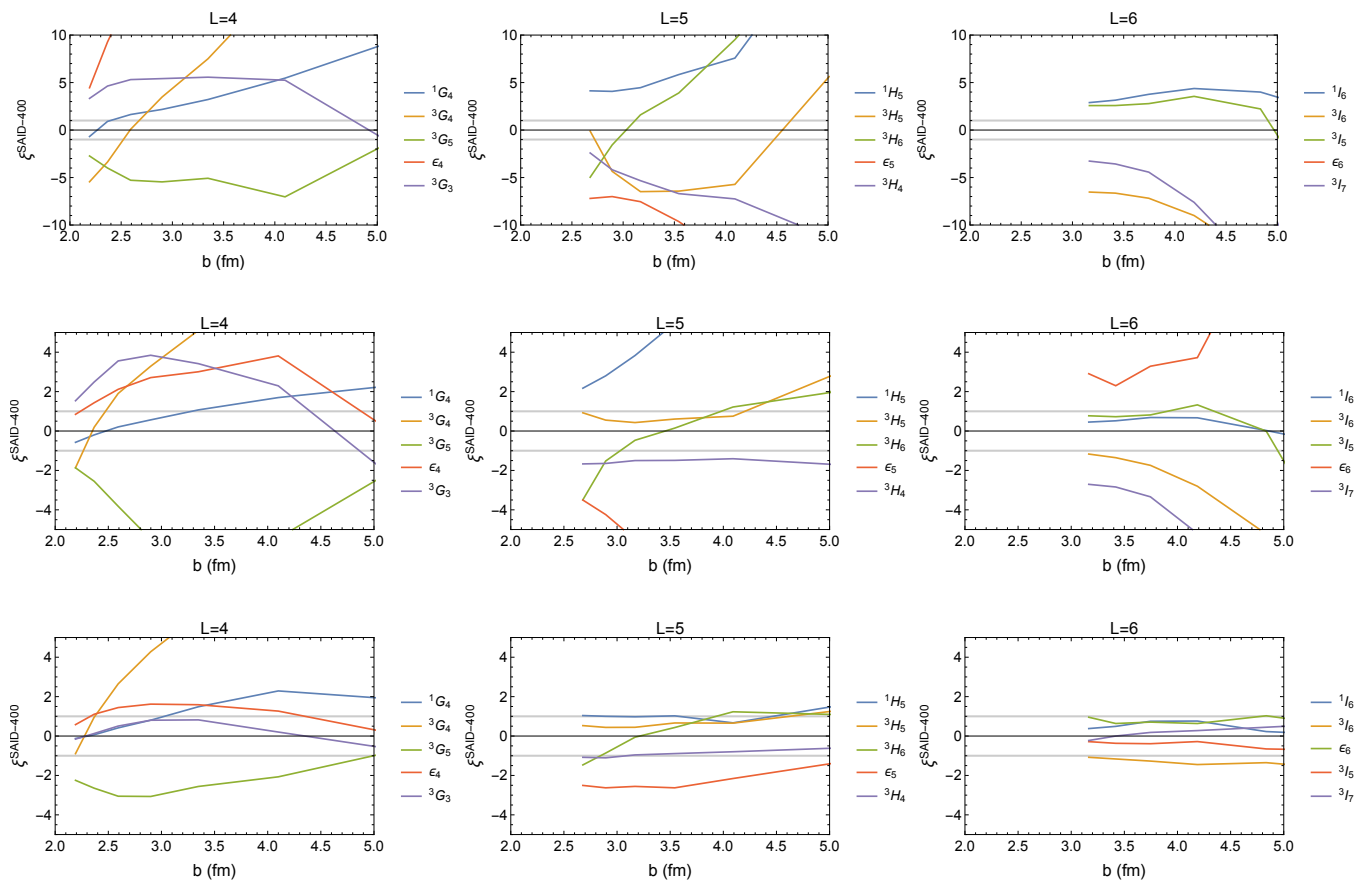


FIG. 8. Same as Fig. 7 for the SAID NN solution in the range 0 – 400 MeV (SP40) [47].

plemented by long distance components described by multiple pion exchange and short distance components, termed counter-terms, which are fitted to scattering data. For a given order in the chiral expansion there is a sufficiently high partial wave where results are finite and counter-term free⁷. Within that scheme, peripheral nucleon-nucleon phase-shifts and chiral symmetry have been confronted [27], and the role of delta excitation, correlated two pion and vector meson exchanges [28, 52] have been analyzed (see also [29] and [30]). The most recent bench-marking study on peripheral nucleon-nucleon scattering goes up to fifth order of chiral perturbation theory [31], and it confronts to the GWU results. One of the appealing features of the power counting is that up to a given order in the chiral expansion peripheral waves are counter-term free. In the case of N5LO this starts with F -waves, i.e. $L \geq 3$. No error bars are included in the N5LO calculation, although they might be inferred from the truncation errors in the expansion.

The N5LO results are compared in Fig. 9 with the Granada phase-shifts as well as with the 13 potentials considered in

this work sharing the *same* CD-OPE potential tail. As we see while some N5LO partial waves deviations are within one sigma, some discrepancies larger than 2–3 sigmas can be also seen, especially for the most peripheral ones. However, the N5LO peripheral phase-shifts become more compatible when the full set of phase-shifts is considered, as it can be observed from the bottom panels of Fig. 9. Thus, the validation of N5LO requires admitting that the systematic errors in the phase-shifts are provided by the spread in the 13 PWA set.

A global view of this spreading of phase-shifts is provided in Fig. 10 in the conventional representation where we provide the 1σ confidence bands computed from Eqs. (23) and (24). Remarkably, the authors of the N5LO calculation carried out the comparison with the SAID result only, which, in view of our plots, is not the best choice.

VI. CONCLUSIONS

In the present paper we have conducted a comprehensive study of the peripheral properties of NN interactions below 350 MeV, focusing in the design of quantitative tests assessing the long-distance quality of a given analysis. This approach has the advantage that we may visualize the effective probing range of the different partial waves in a fewer number of plots. They have been systematically classified in the

⁷ That means that the short range piece of the potential $V_{\text{Short}}(r)$ can be set to zero in that partial wave within uncertainties, see e.g. the discussion in Ref. [36]

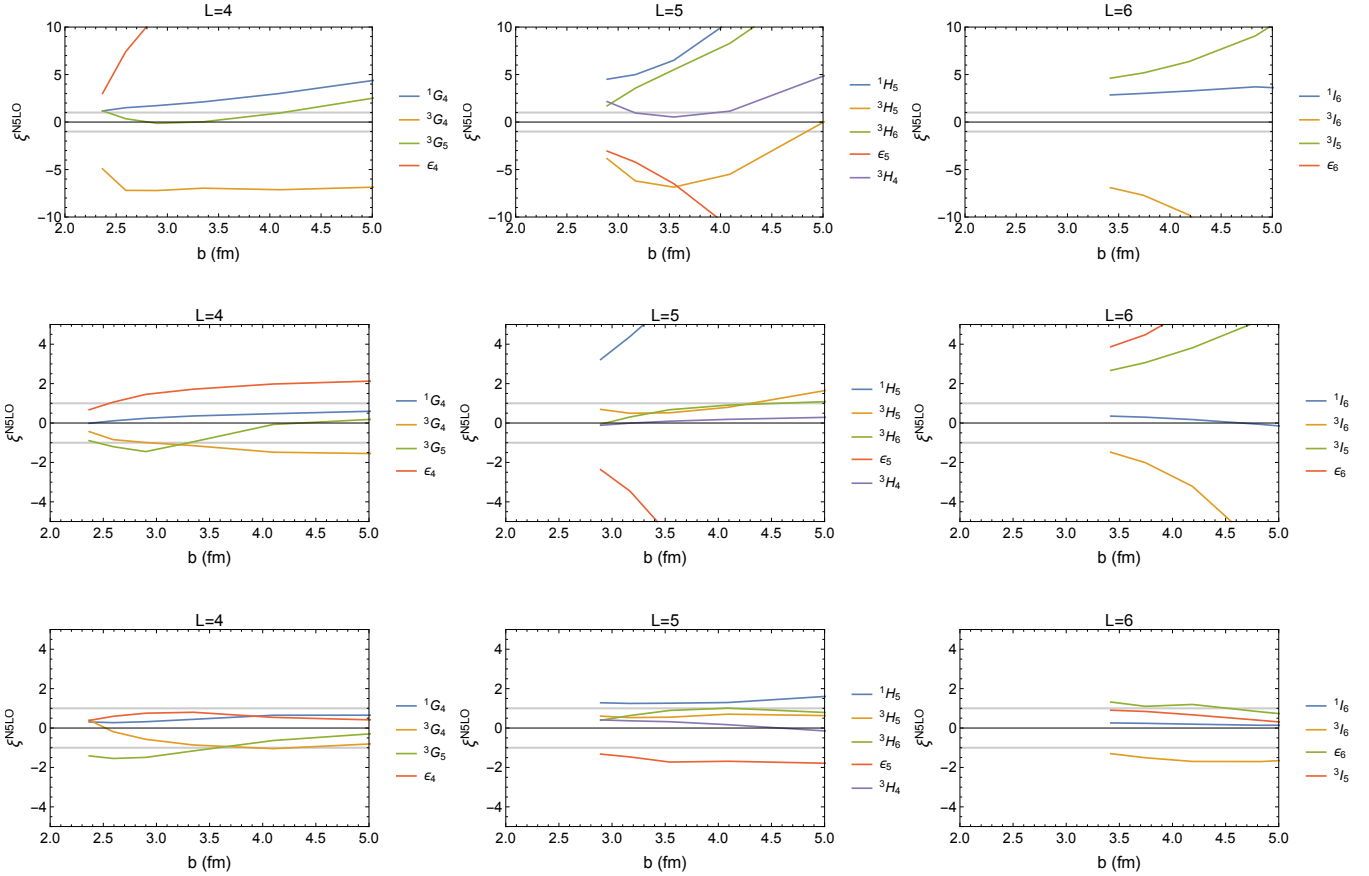


FIG. 9. Same as Fig. 7 for the N5LO chiral perturbative calculation of Entem *et al.*, [31].

so called peripheral plot. This has allowed us to find a high degree of universality in different partial waves sharing the same CD-OPE potential tail. This required to compute the scaled phase-shift $(L + 1/2)\delta_L(p)$, which should become an universal function of the impact parameter $b = (L + 1/2)/p$ for large L peripheral waves. It also implies exploring large values of the impact parameter, linked to the long range behavior of the NN interaction. We also find this peripheral plot to be specially suited for discussing uncertainties and testing new interactions not based on a CD-OPE potential and having a high statistical quality.

Using 13 high-quality sets of phase-shifts, starting from the early Nijmegen-1993 database and covering up to the most recent Granada-2013 one, we have analyzed their scaling properties for large b . All these 13 analyses own their high-quality character to the fact that they share the same CD-OPE potential in coordinate space and include all needed electromagnetic effects. If we take the spread of all 13 analyses as a measure of the systematic error, the peripheral scaling works fairly well.

Finally we have performed three peripheral tests for two recent sets of phase-shifts, which do not enjoy the high-quality character, based on the normalized discrepancies with three sets involving high-quality analyses. The first test corresponds to the original DS-OPE potential used to select the Granada-2013 database, giving the most accurate fit to the largest NN-

scattering data-set up to date. The second test comprises the mean and standard deviation with respect to the 6 Granada-2013 potentials. Finally, the third test includes all 13 high-quality fits carried out since the Nijmegen analysis in 1993.

On one hand, we have tested the peripheral structure of the SAID analysis comprising the largest number of NN scattering data that has been analyzed to date, and going up to 3 GeV and 1.3 GeV for pp and np data, respectively. This analysis does not contain the high-quality long-distance features and, as expected, it fails most of the peripheral tests. Therefore, the SAID phases are not well-suited for accurate comparisons below pion production threshold.

On the other hand, we consider the recent peripheral analysis within chiral perturbation theory to fifth order (N5LO) in the expansion. Here, the peripheral phases have been computed without any fit to NN scattering, and the couplings entering the calculation are taken from πN scattering. Thus, they can be regarded as pure predictions of the NN interaction for long distances, hence their theoretical interest. While we share the view that the rough and visual agreement with the PWA phase-shifts is already encouraging, some deviations with respect to the high-quality potentials are large enough to question the convergence of the expansion. A comparison with statistical and systematic errors obtained by the latest fits using the Granada-2013 database provide a complete falsification of these interactions. The validation of this ap-

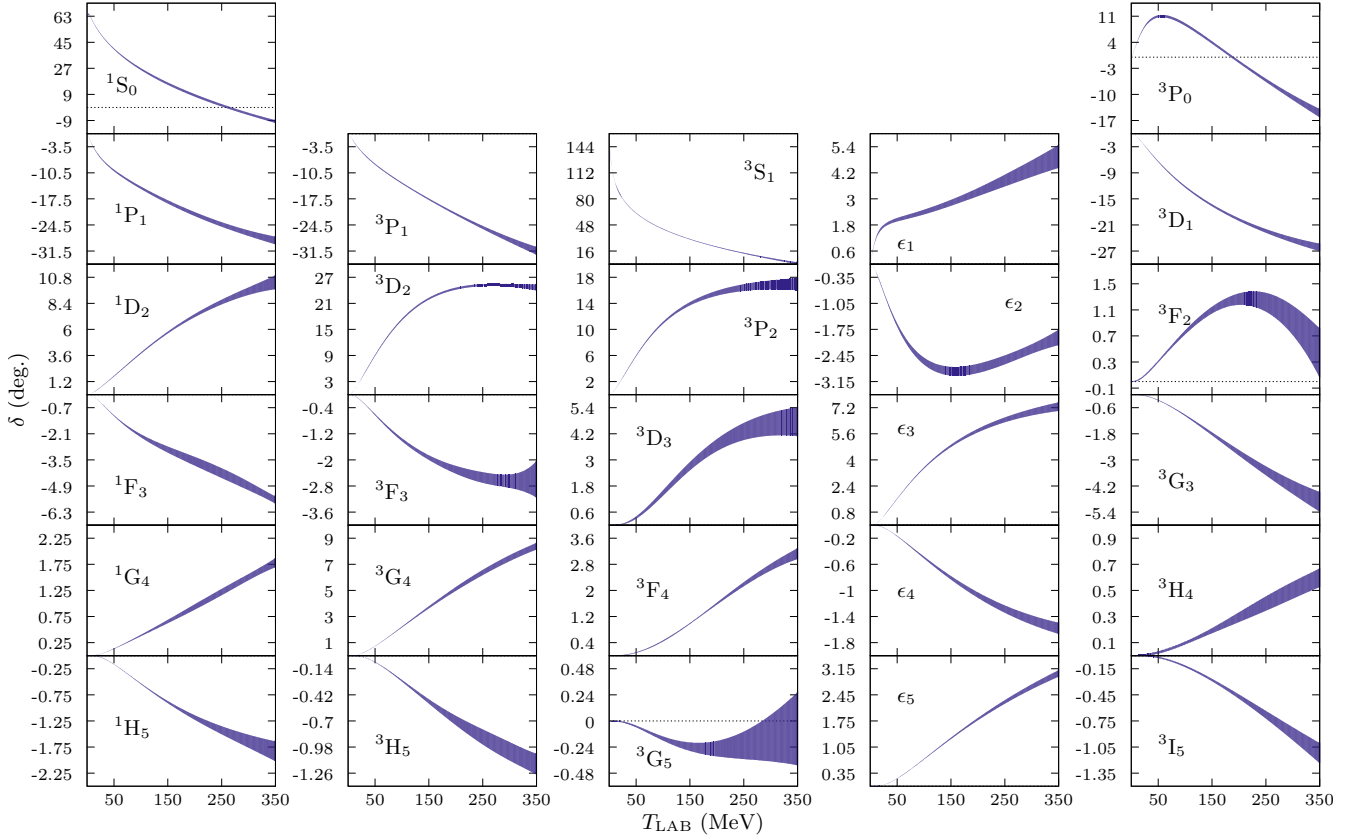


FIG. 10. Same as Fig. 1 but with the band given by 1σ confidence level. See main text.

proach would require assuming that the dominating errors in the phase-shifts are given by the average of all 13 high-quality post-Nijmegen 1993 analyses, as summarized in Fig. 10.

Our findings have an impact on the predictive power of nuclear structure calculations and the validation or falsification of nuclear forces (see e.g. Ref. [37] and references therein). The basic point is that peripheral waves are not only determined to much better accuracy than the low-lying partial waves needed for nuclear structure calculations, but they are essential to remove systematic errors and to achieve an acceptable statistical confidence level on the PWA. A failure in the peripheral test beyond reasonable levels would correspond to an arbitrary enlargement of the peripheral waves uncertainties with a much larger effect on the low partial waves.

VII. ACKNOWLEDGEMENTS

We thank R. Machleidt for sending us the G, H and I peripheral waves phase-shifts for the perturbative N5LO chiral interaction and the CD Bonn ones.

This work is supported by Spanish Ministerio de Economía y Competitividad and European FEDER funds (Grants No. FIS2014-59386-P and FIS2017-85053-C2-1-P), the Agencia de Innovación y Desarrollo de Andalucía (Grant No. FQM225), the U.S. Department of Energy by Lawrence Livermore National Laboratory under Contract No. DE-AC52-

07NA27344, U.S. Department of Energy, Office of Science, Office of Nuclear Physics under Award No. de-sc0008511 (NUCLEI SciDAC Collaboration). I.R.S. acknowledges financial support from MINECO (Spain) under contract No. IJCI-2014-20038 (Juan de la Cierva-Incorporación program).

Appendix A: Convergence of the partial wave expansion

We analyze the convergence of the partial wave expansion for a spherical well potential of range a and strength U_0 . The phase-shifts are well-known and they are given by log-matching the inner and outer reduced wave functions at the point $r = a$.

$$u_{\text{in}}(r) = \hat{j}_L\left(\sqrt{p^2 + U_0}r\right) \quad r < a, \quad (\text{A1})$$

$$u_{\text{out}}(r) = \hat{j}_L(pr) - \tan \delta_L(p) \hat{y}_L(pr) \quad r > a, \quad (\text{A2})$$

Here $\hat{j}_L(x) \equiv x j_L(x)$ are the reduced spherical Bessel functions, and the same applies for the second kind ones $\hat{y}_L(x)$. A sample result is presented in Fig. 11 for the phase-shifts and the corresponding peripheral plot compared with the eikonal approximation. We see that while $\delta_L(p) \approx 0$ for $L \gtrsim pa$, the peripheral plot shows some diffractive effect since $\Delta_L(b) = (L + \frac{1}{2})\delta_L(b)$ does not vanish at $b \gtrsim a$ but at a somewhat larger value. For comparison we also depict the eikonal approximation.

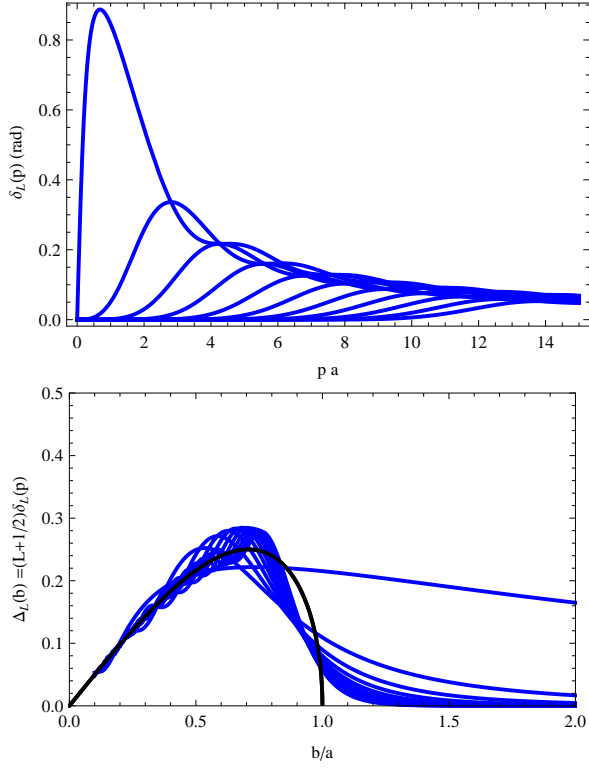


FIG. 11. Phase-shifts (upper panel) and the corresponding peripheral plot (lower panel) for $l = 0, \dots, 10$ (thin solid lines) for an attractive spherical well with strength $U_0 = 2$ and range $a = 1$ (in arbitrary units). We also show the eikonal approximation (thick solid black line).

In Fig. 12 we also display the convergence of the partial wave expansion for several angles and momenta. One can observe that the maximal value of the angular momentum (L_{\max}) which is necessary to be reached in order to saturate the partial wave expansion, depends on the scattering angle. Generally, it ranges from $L_{\max} = pa$ to $L_{\max} = 2pa$ for backward angles.

Appendix B: Perturbative OPE potential

The early perturbative treatment of Wu and Ashkin [53] (see also [54]) is rather involved and we proceed here differently. Actually, a direct derivation of perturbation theory can be easily achieved by starting with the system of coupled channel radial equations (we omit the S, J dependence)

$$-u''_{p,l}(r) + \frac{l(l+1)}{r^2} u_{p,l}(r) + \sum_{l'} U_{l,l'}(r) u_{p,l'}(r) = p^2 u_{p,l}(r), \quad (\text{B1})$$

where $U_{l',l} = 2\mu V_{l'l}$. We can effectively transform this into an equivalent system of integral equations

$$u_{p,l}(r) = \hat{j}_l(pr) + \int_0^\infty dr' G_l(r,r') \sum_{l'} U_{l,l'}(r') u_{p,l'}(r'), \quad (\text{B2})$$

where $G_l(r,r')$ is the Green's function of Eq. (B1), given by

$$pG_l(r,r') = \hat{j}_l(pr_<) \hat{y}_l(pr_>), \quad (\text{B3})$$

with $r_< = \min\{r,r'\}$ and $r_> = \max\{r,r'\}$.

In the case of OPE the potential reads

$$V_{\text{OPE}}(r) = \tau_1 \cdot \tau_2 [\sigma_1 \cdot \sigma_2 W_S(r) + S_{12} W_T(r)], \quad (\text{B4})$$

and we have that the $V_{L,L'}^{JS}(r)$ matrix elements are non-vanishing for $J = L$ and $(S,P) = (0, (-1)^L)$, $J = L$ and $(S,P) = (1, (-1)^J)$ and $L = J \pm 1$ for $(S,P) = (1, (-1)^{L+1})$ and fulfilling $(-1)^{L+S+T} = -1$. These potential matrix elements are given by

$$V_{J,J}^{J0}(r) = \tau(-3)W_S(r) \quad (\text{B5})$$

$$V_{J,J}^{J1}(r) = \tau [W_S(r) + 2W_T(r)], \quad (\text{B6})$$

$$V_{J+1,J+1}^{J1}(r) = \tau \left[W_S(r) - \frac{2(J+2)}{2J+1} W_T(r) \right], \quad (\text{B7})$$

$$V_{J-1,J-1}^{J1}(r) = \tau \left[W_S(r) - \frac{2(J-1)}{2J+1} W_T(r) \right], \quad (\text{B8})$$

$$V_{J+1,J-1}^{J1}(r) = \tau \frac{6\sqrt{J(J+1)}}{2J+1} W_T(r), \quad (\text{B9})$$

where $\tau = \tau_1 \cdot \tau_2 = -3, 1$ for $T = 0, 1$, respectively.

The reaction matrix is given by

$$R_{l',l}^{JS}(p',p) = \frac{1}{p'p} \int_0^\infty dr \hat{j}_{l'}(p'r) 2\mu V_{l',l}^{JS}(r) u_{p,l}^{JS}(r). \quad (\text{B10})$$

In the nuclear bar representation the S-matrix reads,

$$S^{J1} = \begin{pmatrix} e^{i\bar{\delta}_{J-1,J-1}^{J1}} & 0 \\ 0 & e^{i\bar{\delta}_{J+1,J+1}^{J1}} \end{pmatrix} \begin{pmatrix} \cos 2\bar{\epsilon}_J & i \sin 2\bar{\epsilon}_J \\ i \sin 2\bar{\epsilon}_J & \cos 2\bar{\epsilon}_J \end{pmatrix} \times \begin{pmatrix} e^{i\bar{\delta}_{J-1,J-1}^{J1}} & 0 \\ 0 & e^{i\bar{\delta}_{J+1,J+1}^{J1}} \end{pmatrix}. \quad (\text{B11})$$

From here we define the T-matrix

$$S^{JS} = 1 - 2ipT^{JS}, \quad (\text{B12})$$

and the on-shell reaction matrix R (for $p' = p$)

$$R_J^{-1} = T_J^{-1} - ip. \quad (\text{B13})$$

In the limit of small phases, $\bar{\epsilon}_J, \bar{\delta}_J \rightarrow 0$, we get

$$R_J = -\frac{1}{p} \begin{pmatrix} \bar{\delta}_{J-1,J-1}^{JS} & \bar{\epsilon}_J \\ \bar{\epsilon}_J & \bar{\delta}_{J+1,J+1}^{JS} \end{pmatrix} + \dots \quad (\text{B14})$$

Using this form and the perturbative series for the wave function we get (again for $p' = p$)

$$R_{l',l}^{JS}(p,p) = \frac{1}{p^2} \int_0^\infty dr \hat{j}_{l'}(pr) 2\mu V_{l',l}^{JS}(r) \hat{j}_l(pr) + \mathcal{O}(V^2), \quad (\text{B15})$$

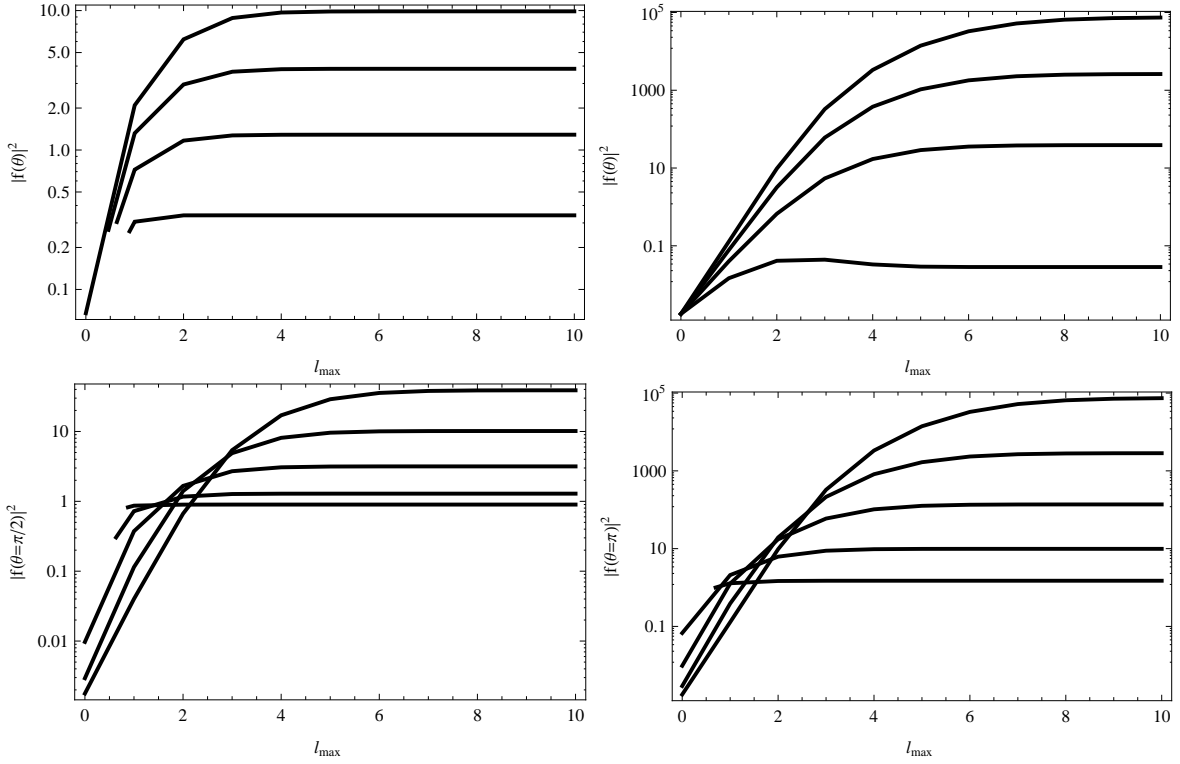


FIG. 12. Convergence of the partial wave expansion for an attractive spherical well with strength $U_0 = 2$ and range $a = 1$ (in arbitrary units) as a function of the maximal angular momentum L_{\max} . Upper panel: $p = 2$ (left) and $p = 5$ (right) from top to bottom $\theta = \pi, 3\pi/4, \pi/2, \pi/4$. Lower panel: $\theta = \pi/2$ (left) and $\theta = \pi$ (right) from top to bottom $p = 5, 4, 3, 2, 1$.

whence Eqs. (15), (16) and (17) follow. The corresponding integrals were determined in Refs. [22–24] and for completeness we quote here the corresponding expressions for the scaled phase-shifts⁸

$$\Delta_J^{S=0} = \tau \frac{Mpf^2}{2m^2} (2J+1)(z-1)Q_J(z), \quad (\text{B16})$$

$$\Delta_{L=J}^{S=1} = \tau \frac{Mpf^2}{2m^2} [-(J+1)Q_{J-1}(z) + (2J+1)Q_J(z) - JQ_{J+1}(z)], \quad (\text{B17})$$

$$\Delta_{SLJ}^- = \tau \frac{Mpf^2}{2m^2} [Q_{J-1}(z) - Q_J(z)] \frac{(2J-1)}{(2J+1)}, \quad (\text{B18})$$

$$\Delta_{SLJ}^+ = \tau \frac{Mpf^2}{2m^2} [Q_J(z) - Q_{J+1}(z)] \frac{(2J+3)}{(2J+1)}, \quad (\text{B19})$$

$$\Delta_{SLJ}^\varepsilon = -\tau \frac{Mpf^2}{2m^2} \sqrt{J(J+1)} [Q_{J-1}(z) - 2Q_J(z) + Q_{J+1}(z)], \quad (\text{B20})$$

where $Q_J(z)$ are the Legendre functions and $z = 1 + m^2/2p^2$. These functions have branch points at $z = \pm 1$ so that the branch cut must be specified. Here, we just take the unambiguous real part.

⁸ There is a typo in Ref. [24] which, however, has no consequences in the final formula

Appendix C: Scaled phase-shifts in the WKB approximation

We proceed by using the WKB representation of the reduced spherical Bessel functions, as an approximation to the free wave solutions in the classically allowed region, i.e. for $r > r_0$, with r_0 a turning point of the classical trajectory. This WKB representation can be written as

$$\hat{j}_{L,\text{WKB}}(r) = \sqrt{\frac{p}{p_L(r)}} \sin \left[\int_{r_0}^r p_L(r') dr' + \frac{\pi}{4} \right], \quad (\text{C1})$$

where the free local momentum is only modified by the centrifugal barrier, and tends to the asymptotic momentum p for $r \rightarrow \infty$. Its expression is given by

$$p_L(r) = \sqrt{p^2 - \frac{(L+1/2)^2}{r^2}} \equiv p \sqrt{1 - \frac{b^2}{r^2}}, \quad (\text{C2})$$

where the semi-classical expression $pb = L + \frac{1}{2}$ has been used to introduce the impact parameter in the last step of Eq. (C2). Thus, the classical turning point, r_0 , can be naturally identified with the impact parameter b , as this is the point on the classical trajectory that satisfies $p_L(r_0) = 0$. In Eq. (C2) we have also included Langer's modification $L(L+1) \rightarrow (L+1/2)^2$, in order to implement the correct short distance asymptotic behavior in the classically forbidden region $r < b$.

The integral of the local momentum appearing in Eq. (C1)

can be identified with the classical action and its result is

$$S_L(r) = \int_b^r dr' p \sqrt{1 - \frac{b^2}{r'^2}} = p\sqrt{r^2 - b^2} - pb \arccos\left(\frac{b}{r}\right). \quad (\text{C3})$$

Finally, to obtain Eq. (21) for the scaled phase-shifts in the WKB approximation, it is necessary to substitute the WKB representation of the free wave solutions, given by eq. (C1), into Eqs. (15) and (16) for the diagonal phase-shifts

$$\delta_{SLJ}^{\pm}(p)|_{\text{WKB}} = -\frac{M}{p} \int_0^{\infty} dr V_{\pm 1, J \pm 1}^J(r) \frac{r}{\sqrt{r^2 - b^2}} \times \sin^2\left(S_L(r) + \frac{\pi}{4}\right). \quad (\text{C4})$$

The last step corresponds to use the standard WKB rule to replace the square of the oscillating function by its average value $\sin^2 x \rightarrow 1/2$, which finally yields Eq. (21) for the scaled phase-shifts. Note also that the lower limit in the integral (C4) is changed from 0 to b in order to make sense. Indeed, this is related to the fact that the WKB approximation to the free wave solution, Eq. (C1), is only valid in the classically allowed region, i.e., for $r > b$.

In the case of the mixing phase-shift, notice that Eq. (17) corresponds to two different Bessel functions. When substituting the WKB representation of the free solutions, Eq. (C1), the product of two sine functions with different classical ac-

tions arise. Then, we can use the trigonometric identity

$$\sin\left[S_{J-1} + \frac{\pi}{4}\right] \sin\left[S_{J+1} + \frac{\pi}{4}\right] = \frac{1}{2} \cos[S_{J-1} - S_{J+1}] - \frac{1}{2} \cos\left[S_{J-1} + S_{J+1} + \frac{\pi}{2}\right] \quad (\text{C5})$$

The sum of actions in the limit of large J is a large phase and produces an oscillating cosine function whose average value under the integral sign is zero.

$$S_{J+1} + S_{J-1} \approx 2S_J. \quad (\text{C6})$$

The difference of actions, however, yields a finite contribution

$$\cos[S_{J-1} - S_{J+1}] \approx \cos\left[2\arccos\left(\frac{b}{r}\right)\right] = \frac{2b^2 - r^2}{r^2}, \quad (\text{C7})$$

which makes sense if $r > b$.

In this way, the product of two reduced spherical Bessel functions with different orders can be approximated under the integral sign by

$$\begin{aligned} & \sqrt{\frac{p}{p_{J-1}}} \sin\left[S_{J-1} + \frac{\pi}{4}\right] \sqrt{\frac{p}{p_{J+1}}} \sin\left[S_{J+1} + \frac{\pi}{4}\right] \rightarrow \\ & \rightarrow \frac{p}{p_J(r)} \frac{2b^2 - r^2}{2r^2} = \frac{2b^2 - r^2}{2r\sqrt{r^2 - b^2}}, \end{aligned} \quad (\text{C8})$$

and then the scaled mixing phase-shift $\Delta_{SLJ}^{\epsilon}(b)|_{\text{WKB}}$, given by Eq. (22), is obtained.

-
- [1] G. Breit, Rev. Mod. Phys. 34 (1962) 766.
[2] R. Arndt and M. Macgregor, Methods in Computational Physics 6 (1966) 253.
[3] P. Signell, The nuclear potential, Advances in nuclear physics, pp. 223–294, Springer, 1969.
[4] V. G. J. Stoks, R. A. M. Klomp, M. C. M. Rentmeester and J. J. de Swart, Phys. Rev. C **48**, 792 (1993).
[5] V. Stoks et al., Phys.Rev. C49 (1994) 2950.
[6] R.B. Wiringa, V. Stoks and R. Schiavilla, Phys.Rev. C51 (1995) 38.
[7] R. Machleidt, Phys.Rev. C63 (2001) 024001.
[8] F. Gross and A. Stadler, Phys.Rev. C78 (2008) 014005.
[9] V. Stoks and J. J. de Swart, Phys. Rev. C **47**, 761 (1993).
[10] V. G. J. Stoks and J. J. de Swart, Phys. Rev. C **52**, 1698 (1995)
[11] R. Navarro Pérez, J.E. Amaro and E. Ruiz Arriola, Phys. Rev. C88 (2013) 064002. [Erratum: Phys. Rev.C91,no.2,029901(2015)].
[12] R. Navarro Pérez, J.E. Amaro and E. Ruiz Arriola, Phys.Rev. C88 (2013) 024002.
[13] R. Navarro Pérez, J.E. Amaro and E. Ruiz Arriola, Phys.Rev. C89 (2014) 024004.
[14] R. Navarro Perez, J. Amaro and E. Ruiz Arriola, Few Body Syst. 55 (2014) 983.
[15] R. Navarro Pérez, J.E. Amaro and E. Ruiz Arriola, Phys.Rev. C89 (2014) 064006.
[16] R. Navarro Perez, J.E. Amaro and E. Ruiz Arriola, J. Phys. G43 (2016) 114001.
[17] E. Ruiz Arriola, J.E. Amaro and R. Navarro Pérez, Mod. Phys. Lett. A31 (2016) 1630027.
[18] R. Navarro Pérez, J.E. Amaro and E. Ruiz Arriola, Phys.Rev. C95 (2017) 064001.
[19] Sinya AOKI for HAL QCD, S. Aoki, Prog. Part. Nucl. Phys. 66 (2011) 687.
[20] S. Aoki, Eur. Phys. J. A49 (2013) 81.
[21] L. Okun and I.Y. Pomeranchuk, Nuclear Physics 10 (1959) 492.
[22] P. Signell, Progress of theoretical physics 22 (1959) 492.
[23] P. Cziffra et al., Phys. Rev. 114 (1959) 880.
[24] G. Breit and M. Hull, Nuclear Physics 15 (1960) 216.
[25] J. Binstock and R. Bryan, Phys.Rev. D4 (1971) 1341.
[26] S. Weinberg, Phys.Lett. B251 (1990) 288.
[27] N. Kaiser, R. Brockmann and W. Weise, Nucl.Phys. A625 (1997) 758.
[28] N. Kaiser, S. Gerstendorfer and W. Weise, Nucl.Phys. A637 (1998) 395.
[29] E. Epelbaum, W. Gloeckle and U.G. Meissner, Eur.Phys.J. A19 (2004) 125.
[30] H. Krebs, E. Epelbaum and U.G. Meissner, Eur.Phys.J. A32 (2007) 127.
[31] D. R. Entem, N. Kaiser, R. Machleidt and Y. Nosyk, Phys. Rev. C 91 (2015) no.1, 014002

- [32] R. Navarro Perez, J. E. Amaro and E. Ruiz Arriola, Prog. Part. Nucl. Phys. **67**, 359 (2012)
- [33] R. Navarro Pérez, J. E. Amaro and E. Ruiz Arriola, Phys. Lett. B **724**, 138 (2013)
- [34] P. Pascual and A. Galindo, Quantum Mechanics. Vol. I (1990) and vol. II (1991) (Springer-Verlag, Berlin.).
- [35] R. Navarro Pérez, J.E. Amaro and E. Ruiz Arriola, PoS CD12 (2013) 104.
- [36] R. Navarro Perez, J.E. Amaro and E. Ruiz Arriola, Phys. Rev. C91 (2015) 054002.
- [37] E. Ruiz Arriola, J.E. Amaro and R.N. Perez, 12th Conference on Quark Confinement and the Hadron Spectrum (Confinement XII) Thessaloniki, Greece, August 28-September 2, 2016, 2016, EPJ Web Conf. 137 (2017) 09006.
- [38] S.J. Wallace, Annals Phys. 78 (1973) 190.
- [39] M. Pavon Valderrama and E. Ruiz Arriola, Phys. Rev. C74 (2006) 054001.
- [40] M. Pavon Valderrama and E. Ruiz Arriola, Phys. Rev. C 74 (2006) 064004. Erratum: [Phys. Rev. C 75 (2007) 059905].
- [41] J. Besprosvany, Physical Review A 55 (1997) 3539.
- [42] R.S. Christian and E.W. Hart, Physical Review 77 (1950) 441.
- [43] R.A. Arndt et al., Phys. Rev. D28 (1983) 97.
- [44] R.A. Arndt, J.S. Hyslop and L.D. Roper, Phys. Rev. D35 (1987) 128.
- [45] R.A. Arndt et al., Phys. Rev. D45 (1992) 3995.
- [46] R.A. Arndt et al., Phys. Rev. C56 (1997) 3005.
- [47] R.A. Arndt, I.I. Strakovsky and R.L. Workman, Phys. Rev. C62 (2000) 034005.
- [48] R.A. Arndt et al., Phys. Rev. C76 (2007) 025209.
- [49] <http://gwdac.phys.gwu.edu>, Center For Nuclear Studies. Data Analysis center. N-N interaction.
- [50] R. L. Workman, W. J. Briscoe and I. I. Strakovsky, Phys. Rev. C 94 (2016) no.6, 065203.
- [51] R. Machleidt and D.R. Entem, Phys. Rept. 503 (2011) 1, 1105.2919.
- [52] D.R. Entem and R. Machleidt, Phys. Rev. C66 (2002) 014002.
- [53] J. Ashkin and T.Y. Wu, Physical Review 73 (1948) 973.
- [54] T.Y. Wu and T. Ohmura, Quantum theory of scattering, (1962) (Prentice-Hall, Englewood Cliffs, N.J.).